International Journal of Architectural, Civil and Construction Sciences
ISSN: 2415-1734
Vol:7, No:3, 2013

Finite Element Study of a DfD Beam-Column Connection

Zhi Sheng Lin, K. C. G. Ong, Lado Riannevo Chandra, Bee Hong Angeline Tan, Chat Tim Tam, and Sze Dai Pang

***Abstract*—**Design for Disassembly (DfD) aims to reuse the structural components instead of demolition followed by recycling of the demolition debris. This concept preserves the invested embodied energy of materials, thus reducing inputs of new embodied energy during materials reprocessing or remanufacturing. Both analytical and experimental research on a proposed DfD beam-column connection for use in residential apartments is currently investigated at the National University of Singapore in collaboration with the Housing and Development Board of Singapore. The present study reports on the results of a numerical analysis of the proposed connection utilizing finite element analysis. The numerical model was calibrated and validated by comparison against experimental results. Results of a parametric study will also be presented and discussed.

***Keywords*—**Design for Disassembly (DfD), finite element analysis, parametric study.

I. Introduction

TODAY, there is a shortage of sustainable supplies of good quality construction materials to meet the needs of a growing world population and fast pace global urban development. What is perhaps more critical is that buildings are commonly demolished and rebuilt after a short period of service due to redevelopment and their inability to meet the needs of new owners and occupants. This has resulted in wastage of materials and the invested embodied energy of the materials as well as pollution generation. Thus it is become increasingly important to find a more sustainable construction method in the construction industry nowadays. Design for Disassembly (DfD) emerged in the 1990s and has been reported as the most direct approach to increase building material reusability [1]-[5]. The concept aims to reuse the structural components instead of demolition followed by recycling of the demolition debris. Adoption of DfD in the building industry can significantly reduce pollution impacts and increase resource and economic efficiency as instead of demolition and disposal of demolition debris as landfill, the structural components can be disassembled and reused in the new buildings. In essence, the structural components may have two or more phases of service life as long as they are assessed to be satisfactory for further applications.

The design of connections that are demountable is an important consideration in any DfD building systems. Literature is available on a number of innovative DfD building systems utilizing demountable connections since 1970's. Examples include the demountable roof of Munich's airport by means of dowels with threaded rods to form demountable connections between the columns and roof girders in the 1970s, a skeletal and panel system using special fasteners to form pinned connections in the 1980s [6], demountable multiple-level system using post tensioning tendons to tie different module sets in the United States [7], and several demountable column-slab system in the Netherlands [8]. However, the reported systems adopted main connections which were essentially pinned connections possessing little or no moment-resisting capacity when adopted in the structural frames. DfD beam-column connections capable of providing moment-resisting capacity are relatively uncommon.

Research on a feasible DfD building system for use in residential apartments is underway at the National University of Singapore in collaboration with the Housing and Development Board of Singapore. As one of the main targets of this research project, a series of DfD beam-column connections has been proposed. Fig. 1 illustrates schematically the proposed connections. Basically, the bolted endplate connection was chosen as one of the key components of the proposed connection. The main bars are welded on the flange of the embedded I-section for anchorage purposes and oversized holes are provided in the endplate to take into account construction tolerance on site. Three different designs, A, B and WP series were proposed. The A series has the height of the embedded I-section extending up to the slab level with no provision for installing continuity tie bars at the top of the embedded I-sections in the DfD beam-column connection in order to increase the moment capacity of the connection. The B series is designed with the height of the embedded I-section extending up to the height of the precast beam or thereabouts allowing for continuity reinforcement to be provided in the cast-in-situ slab above the DfD beam-column connection. The WP-series is similar to the B series except for the inclusion of an extension unit, as shown in Fig. 1, to allow for extension of the span of the beam when the precast beam component is

Zhi Sheng LIN is a PhD candidate at Civil and Environmental Engineering Department, National University of Singapore (email: g0900490@nus.edu.sg).
K. C. G. ONG is an Associate Professor at Civil and Environmental Engineering, National University of Singapore.
L. R. CHANDRA is a research fellow at Civil and Environmental Engineering, National University of Singapore.
B. H. A. TAN is a research staff at Housing and Development Board, Singapore.
C. T. TAM is an Associate Professorial Fellow at Civil and Environmental Engineering, National University of Singapore.
S. D. PANG is an Assistant Professor at Civil and Environmental Engineering, National University of Singapore.

reused.

Full-scale experimental tests have been carried out to investigate the structural behavior of the proposed connections. The experimental tests were designed to test how the proposed beam-column connections perform when subjected to flexural load, up till failure. Thus the performance of the beam and column is not emphasized and the experimental test set-up of a four-point-bending test with the proposed DfD beam-column connection located at mi-span of the test specimen was selected (Fig. 2). In addition, the results of an analytical study through an efficient finite element analysis (FEA) are also presented in this paper. FEA results were calibrated and validated against the experimental data obtained. Analytical modeling enabled further design optimization and a parametric study of the proposed connections to be carried out.

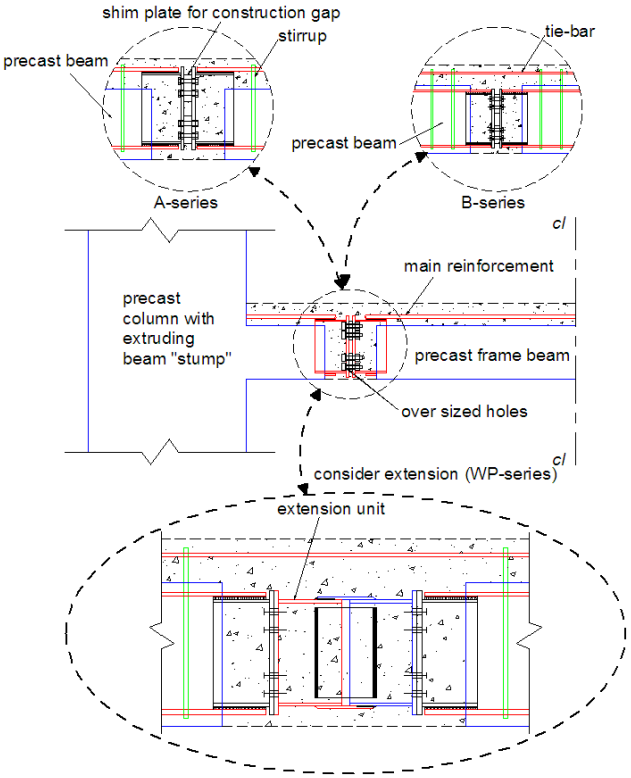

Fig. 1 Principle detail of proposed DfD beam-column connections

II. Experimental Program

Fig. 2 shows the test set-up and instrumentation as adopted in this experimental test program. The results of five full-scale specimens were presented in this paper and compared with the FEA results. The five test specimens corresponding to the three series, viz. A500, A650, B500, B650 and WP650. The specimens were distinguished based on their design detail and dimension of the beam in which the connection is used. Fig. 3 shows the details of the test specimens. In general, the specimens were cast in two layers: the precast beam and cast-in-situ slab. Table I summarizes the typical mechanical properties of the concrete and steel components as used in the test specimens.

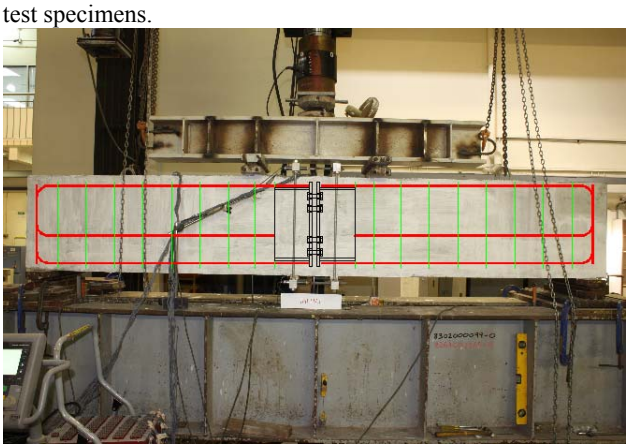

Fig. 2 Four-point-bending test set-up and instrumentation

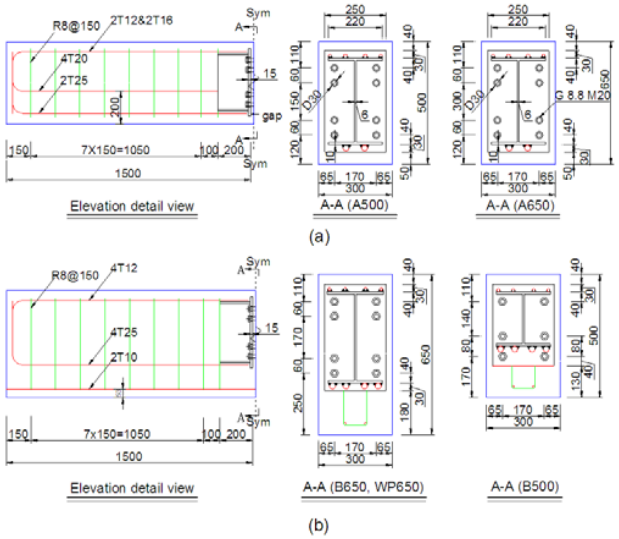

Fig. 3 Detail of the specimens and the proposed DfD beam-column connections (unit mm)

TABLE I
Mechanical Properties of Concrete and Steel Component Parts

Strength of concrete (MPa)			
Type	Compression f_{ck}	Tension* $f_{ctm,fl}$	E_c (GPa)
con(A)-top	40.8	3.4	22.6
con(A)-bot	54.4	3.3	25.4
con(B, WP)-top	34.9	2.6	28.3
con(B, WP)-bot	30.4	2.5	24.1

Strength of steel parts (MPa)			
Type	Elastic modulus	Yield strength	Ultimate strength
Rebar	200×10^3	491	697
Steel plates	200×10^3	296	483
Bolts	200×10^3	640	800

Note: con(A)-top represents concrete at the slab level used in A-series specimens; con(A)-bot represents concrete for the precast beam used in the A-series specimens; con(B, WP)-top represents concrete at the slab level used in the B-series and WP-series specimens; con(recon)-bot represent concrete for the precast beam in the B-series and WP-series; * ASTM E529-04 tests were performed to obtain the concrete flexural strength.

III. Finite Element Simulation

A. Generals

The finite element program ABAQU/Standard was used to model the test specimens. The proposed FEM approach can be summarized as follows:

1) Full bonding at the interface was assumed between the steel components and concrete, i.e. relative slip between the steel and concrete was ignored;
2) The rebar cage and the proposed connection were modeled as a single entity and embedded in the concrete model, thus the degrees of freedom (DOFs) of the nodes of the steel component parts were constrained by the DOFs of the nodes of the surrounding concrete;
3) A general mesh size of 30mm×30mm was adopted for the concrete beam portion and the embedded reinforcement while a finer mesh was applied on the proposed connection, i.e. the size of the elements of the steel plates and bolts was 5mm in the longitudinal direction and 10mm in the vertical direction;
4) Eight-node solid elements with reduced integration (C3D8R) were used to model the concrete beam; four-node shell elements with reduced integration (S4R) were used to model the steel plates; 3D beam element (B31) and 3D truss element (T3D2) were used to model the high strength bolts and rebars, respectively;
5) The welding and bolts assembly (washer, shim plate) were ignored to simplify modeling. The portion of the main reinforcement within the welded anchorage region was modeled using shell elements with the equivalent section area;
6) Elastic-plastic model was used to describe the constitutive relationship of the steel elements such as steel plates, reinforcement and bolts while concrete damage plasticity (CDP) model was used to describe the concrete behavior.

Based on the above mentioned modeling approaches, an integrated and simplified 3D model of the test specimens incorporating the proposed DfD connections was achieved. Instead of using only solid element, several kinds of elements such as solid element, shell element, beam element and truss element were appropriately adopted which make the modeling and analysis more effective.

B. Concrete Model

The CDP model uses the yield function proposed by Lubliner, Oliver et al. [9] and incorporates the modifications proposed by Lee and Fenves [10] to consider different evolutions of concrete strength characteristics under tension and compression.

The constitutive relationship of concrete under compression can be automatically calculated by ABAQUS providing the compression stress-strain relationship of concrete under uniaxial compressive force and some necessary material parameters such as the dilation angle Ψ, ratio of biaxial compression strength and uniaxial compression strength a, eccentricity ε and parameter K_c (the ratio of the second stress invariant on the tensile meridian to that on the compressive meridian). The suggested values of the material parameters in the literature [9]-[13] were adopted as presented in Table II.

TABLE II
Suggested Material Parameters of Concrete Model

Ψ	ε	a (MPa/MPa)	K_c
38°	0.1	1.16	0.667

In this study, the concrete stress-strain relationship under uniaxial compressive load was obtained from concrete cylinder tests. Linear elastic stress in compression was assumed up to $0.4f_{ck}$[14]. Beyond this point, the nonlinear response of concrete could be derived based on the test results according to Eq. 1 and Eq. 2 as per CEB-FIP code [15]. The compressive damage variable can be derived according to Eq. 3.

$$\frac{\sigma_c}{f_{ck}} = -(k\eta - \eta^2)/(1+(k-2)\eta), \text{ for } \left|\varepsilon_c < \varepsilon_{c,\lim}\right|$$

$$\frac{\sigma_c}{f_{ck}} = -\left[\left(\frac{\varepsilon_{cl}}{\varepsilon_{c,\lim}}\xi - \frac{2}{\left(\varepsilon_{c,\lim}/\varepsilon_{cl}\right)^2}\right)\eta^2 + \left(\frac{4\varepsilon_{cl}}{\varepsilon_{c,\lim}} - \xi\right)\right], \quad (1)$$

$$\text{for } \left|\varepsilon_c > \varepsilon_{c,\lim}\right|$$

with,

$$\xi = \frac{4\left[\left(\frac{\varepsilon_{c,\lim}}{\varepsilon_{cl}}\right)^2(k-2) + 2\frac{\varepsilon_{c,\lim}}{\varepsilon_{cl}} - k\right]}{\left[\frac{\varepsilon_{c,\lim}}{\varepsilon_{cl}}(k-2)+1\right]^2}, \quad (2)$$

$$\varepsilon_{c,\lim} = 0.5\left(0.5k+1\right) + \left(0.5\left(0.5k+1\right)^2 - 0.5\right)^{0.5}$$

where,

ε_c is the concrete compression strain;

ε_{cl} is the strain at maximum compressive stress;

k is the ratio between elastic modulus and ultimate modulus;

η $=\varepsilon_c / \varepsilon_{cl}$.

$$d_c = 1 - \exp(-a_c\varepsilon^p), \quad (3)$$

Where,

d_c is the compressive damage variable;

ε^p is the plastic compressive strain;

a_c is material parameter.

The constitutive relationship of concrete under tensile can be automatically calculated in ABAQUS by imputing the stress-strain relationship or stress-crack opening relationship of concrete under uniaxial tension. In this study, the stress-crack opening relationship of concrete was used according to Eq. 4

[15]. The tensile damage variable could be derived as the ratio of the area under the stress-crack opening curve.

$$\sigma_{ct}(w) = f_{ct}\left(1 - 0.8\frac{w}{w_l}\right) \text{ for } w \le w_l$$
$$\sigma_{ct}(w) = f_{ct}\left(0.25 - 0.05\frac{w}{w_l}\right) \text{ for } w_l \le w \le w_c \quad (4)$$

Where,

f_{ct} is the tensile strength of concrete;

w is the crack opening in mm;

$w_l = G_f / f_{ct}$ corresponding to $\sigma_{ct} = 0.2 f_{ct}$;

$w_c = G_f / f_{ct}$ corresponding to $\sigma_{ct} = 0$;

G_f is the concrete tensile fracture energy.

C. Boundary Conditions

The numerical analysis was performed based on displacement control algorithm. The displacement load was applied on the predefined reference point which was coupled with the loading area of the beam in the vertical direction. The supports were modeled using an analytically rigid member. A "frictional contact" was invoked between the specimen and the rigid supports with a friction coefficient of 0.4 [16]. Fig. 4 shows the final numerical model and boundary conditions.

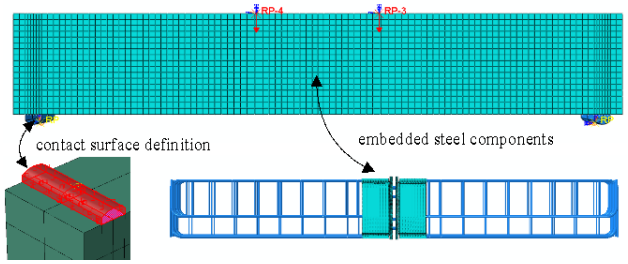

Fig. 4 Finite element model and boundary conditions

IV. Calibration of FEA Results

A. General

The proposed modeling approaches were calibrated by comparisons against the test results to gauge the sensitivity of the modeling parameters adopted. The calibration included investigation of the influence of the concrete element type adopted and the mesh dependency. The test results of the A500 specimen was used for comparison in terms of moment vs. mid-span deflection (M-Δ) curves. The initial modeling as described previously used the C3D8R concrete elements with a mesh size of 30mm×30mm. Fig. 5 shows a comparison of the analytical M-Δ curves between the FEA result and the experimental results. In general, the numerical results show good agreement with the experimental data in terms of overall trend and the ultimate moment capacity prediction.

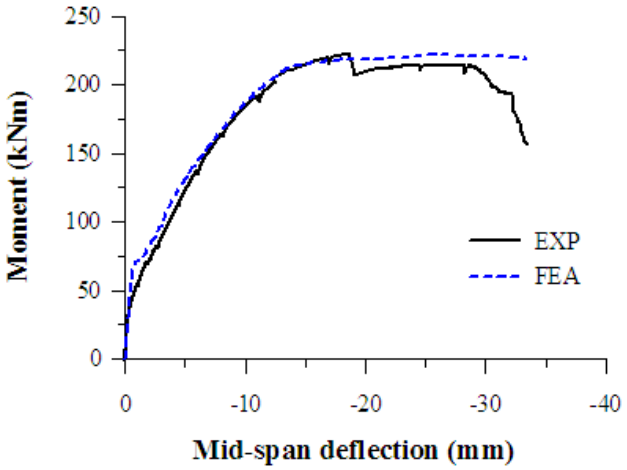

Fig. 5 Comparison of numerical result with experimental result of A500 specimen

B. Influence of Concrete Element Types

Linear solid elements (8 nodes brick elements) and nonlinear solid elements (20 nodes brick elements) are available in ABAQUS software. It is found that when nonlinear solid elements were used, the computational cost of FEA was significantly increased, therefore in this paper the study of influence of concrete element type was mainly focused on the linear solid elements. Three types of linear solid elements are available in ABAQUS. They are 8 nodes brick element with full integration (C3D8), 8 nodes brick element with reduced integration and 8 nodes brick element with compatible mode [17]. The FEA case study with different concrete element types was carried out and the M-Δ curves obtained were compared as shown in Fig. 6. It seemed that the models using C3D8 and C3D8I yielded a slightly stiffer structural response as the applied load increased vis-a-vis the C3D8R model and the experimental results. Comparing computational costs showed that the analysis using C3D8R was more effective. It is worth noting that the element type C3D8I was found to be sensitive to element distortion and thus numerical divergence was encountered, when specimen deflection exceeded 20mm.

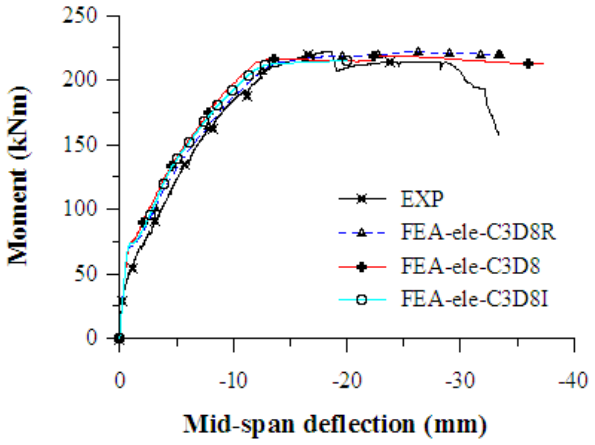

Fig. 6 Influence of concrete element types on the FEA result

C. Influence of Mesh Schemes

Finite element analysis is usually sensitive to mesh schemes (element size and directions). In this section, case studies of finite element analysis adopting various mesh schemes viz. 10mm, 20mm, 30mm, 40mm and 50 mm were conducted.

Fig. 7 shows the FEA results obtained. It is noted that the M-Δ curves results were not especially sensitive to the mesh schemes adopted when the element size was smaller than 30mm due to the fact that fracture energy concept has been used in defining the concrete tensile behavior in the CDP model [17]. However, the model adopting an element size exceeding 30mm yielded an obviously stiffer structural response especially at the state when the specimen displacement was large compared to the experimental results. It may due to the hour-glassing issue when reduced integration element was used [17]. On the other hand, besides yielding almost the same accuracy, using a finer mesh will significantly increase the computational cost of the analysis. Through the mesh sensitivity analysis, a general mesh scheme with an element size of 30mm was deemed to be most cost-effective for the present study.

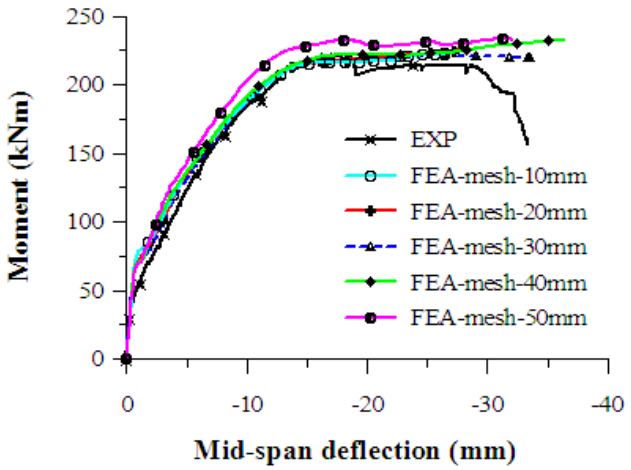

Fig. 7 Influence of general mesh schemes on the FEA results

V. Validation of FEM

To verify the calibrated FEM, the analytical results were compared with the experimental results of the test specimens in terms of ultimate moment capacities as summarized in Table III. It is noted that specimen B500 failed prematurely due to the fracture of the weld between the flange plate and flange plate during testing. Excluding specimen B500, the mean ratio of the experimental results to the analytical results has a value of about 0.99 and a coefficient of variation of about 0.0003. In general, the trend of M-Δ response and ultimate moment capacities of the proposed DfD connections have been well predicted with sufficient accuracy and numerical stability using the proposed FEM approach. A comparison in detail will be discussed in a subsequent journal paper.

TABLE III
Test Results and FEA Results in Terms of Ultimate Moment Capacity

Test specimens	size (mm)	$M_{\max}^{\exp}$	$M_{\max}^{fem}$	$\frac{M_{\max}^{\exp}}{M_{\max}^{fem}}$
A500	300×500	222.1	219.9	1.01
B500	300×500	188.2	201.6	0.93
A650	300×650	310.7	311.2	1.00
B650	300×650	301.8	310.7	0.97
WP650	300×650	280.2	281.8	0.99

VI. Parametric Study

In this section, the results of a parametric study conducted to investigate sensitivity of the structural behavior of the proposed DfD connections to some of the main design parameters are reported. Based on the design formula of an equivalent T-stub bolted endplates connection in EC3 [18], two parameters viz. the endplate thickness and the bolt grade were selected.

A. Influence of Endplate Thickness

The influence of endplate thickness on the structural behavior of the A500 and B500 connections were investigated by varying the endplate thickness viz. 10mm, 15mm, 20mm and 30mm in the four-point-bending. A construction gap of 25mm was assumed to simulate lack of fit in practice which was also recommended as the minimum construction clearance in PCI handbook [19]. Fig. 8 and Fig. 9 show the M-Δ curves of the models with respect to various endplate thicknesses. For the A500 connection specimen, it was found that the M-Δ curves were unaffected during the initial stage of loading and the difference became discernible only after cracking represented by concrete tensile damage occurred at mid span between two end plates of the proposed DfD connection. In general, the structural stiffness of the proposed connection as represented by the gradient of the M-Δ curves was increased with the increase in endplate thickness. However, it is noted that the influence seemed not significant when the endplate thickness was increased from 20mm to 30mm. On the other hand, the ultimate moment capacity of the proposed connection was only slightly affected when the endplate thickness was increased from 15mm to 30mm which may imply that the failure of the proposed connection was also affected by the other parameters such as bolt grade, web plate, and concrete grade etc.

In contrast, in the case of the B500 connection specimens, it is noted that the influence of the endplate thickness on the structural stiffness of the connection was much less significant. It may due to that fact that the height of the endplate in the B500 connection was much smaller than that of the A500 connection. Thus the endplate thickness contributes much less in terms of section stiffness. However, increasing the endplate thickness from 15mm to 20mm resulted in a significant increase in ultimate moment capacity of the B500 connection specimens. On the other hand, the ductile performance of the connection was adversely affected by the increase in the endplate thickness. This was not observed in the A500 connection specimens.

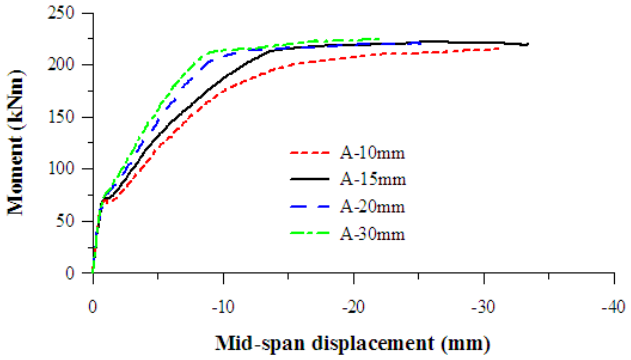

Fig. 8 M-Δ curves of A500 specimens with various endplate thicknesses

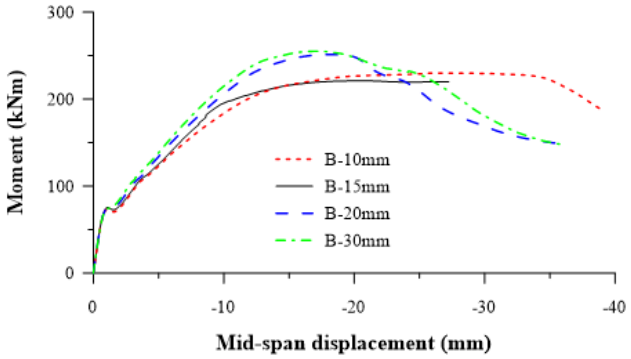

Fig. 9 M-Δ curves of B500 specimens with various endplate thicknesses

B. Influence of Bolt Grade

The influence of bolt grade on the structural behavior of the A500 and B500 connections were investigated in this section by varying the grade of bolt viz. Grade 5.8, Grade 6.8, Grade 8.8 and Grade 10.9. The yield strengths were assumed to be 400, 480, 640 and 900MPa respectively with the ultimate strengths of 500, 600, 800, and 1000MPa, respectively. The maximum strain corresponding to the ultimate strength of the different grade bolts was assumed to be 0.1 and the elastic modulus was assumed to be 200GPa [20]. The fracture percent elongation of the Grade 5.8 and Grade 6.8 bolt was assumed to be 0.20 and the fracture percent elongations of the Grade 8.8 and Grade 10.9 bolt were assumed to be 0.12 and 0.11, respectively according to BS EN ISO 898-1:1999 [21].

Fig. 10 and Fig. 11 show the M-Δ curves of the models with respect to the various bolt grades assumed. It is noted, for the A500 connection specimen, an increase in the bolt grade resulted in a slight increase in the structural stiffness and significant increase in the ultimate moment capacity of the connection when the bolt grade was lower than Grade 8.8. Beyond this, the influence of bolt grade on the ultimate moment capacity of the proposed A500 connection seemed minimal. In addition, from the point of view of failure mode and ductile performance, it is noted that when the bolt grade was lower than Grade 8.8, the failure mode of the proposed A500 connection was governed by failure of the bolts and resulted in a relatively more brittle failure.

For the B500 connection specimen, it is noted that increasing the bolt grade did not affect the structural stiffness of the connection significantly since the bolts were located much further away from the tensile side of the beam vis-a-vis the A500 connection. However, the increase in the bolt grade has resulted in a significant increase in the ultimate moment capacity of the connection. On the other hand, the ductility performance of the connection seemed not to be significantly affected even though it was observed that the bolt failure governed the failure mode of the connection when a lower grade bolt was used (i.e. lower than Grade8.8).

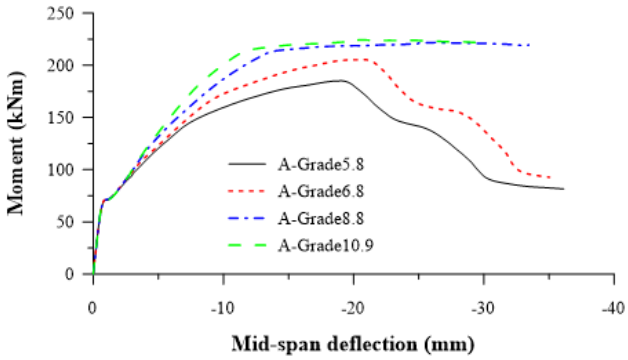

Fig. 10 M-Δ curves of A500 specimens with various bolt grades

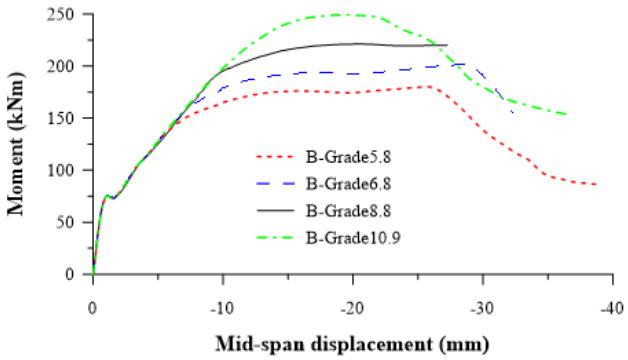

Fig. 11 M-Δ curves of B500 specimens with various bolt grades

VII. Conclusion

A finite element tool was explored for the numerical study of a proposed DfD beam-column connection. The proposed FEM approach was calibrated and validated by comparison against available experimental test results. The validated model was utilized to carry out further parametric study of the proposed DfD connection. Based on the results obtained, several conclusions can be drawn.

1) The proposed finite element modeling approach in this paper was calibrated and validated for modeling the proposed DfD connections.
2) The FEA results seemed not to be especially dependent on the element mesh size due to the fact that the fracture energy concept has been used in defining the concrete

tensile behavior in the CDP model in ABAQUS. However, adoption of an over-coarse element mesh size (i.e. larger than 30mm) may yield a stiffer structural response of the specimen.

3) Eight-node brick elements with reduced integration (C3D8R) in ABAQUS was verified to be more cost-effective in simulating the concrete beam in the analysis with acceptable accuracy compared to when the other two types of eight-node linear brick elements (C3D8 and C3D8I) were used.
4) In general, an increase in the endplate thickness resulted in an increase in the structural stiffness of the proposed A500 connection specimen. However, the ultimate moment capacity seemed to be unaffected when the endplate thickness was increased from 15mm to 30mm. For the B500 connection specimens, an increase in the endplate thickness did not influence the structural stiffness significantly. However, increasing the endplate thickness resulted in a significant increase in the ultimate moment capacity of the B500 connection specimen and a relatively more brittle behavior at failure.
5) Increasing the bolt yield strength only affected the structural stiffness of the A500 connection. However, an increase in the bolt ultimate strength resulted in a significant increase in the ultimate moment capacities of both the A500 connection specimen and the B500 connection specimen. From the point view of ductile behavior, the ductile performance of the A500 connection specimen was adversely affected by an increase in the bolt grade.

REFERENCES

[1] John, VM. (2003), "On the sustainability of concrete" Industry and Environment 26(2):62-63.
[2] Kibert, C. (2003). "Deconstruction: the start of a sustainable materials strategy for the built environment" Industry and Environment 26(2): 84-88.
[3] Pulaski, M. H.(2004) , Field Guide for Sustainable Construction. The Pennsylvania State University.
[4] Guy, B., & Shell, S. (2002). Design for Deconstruction and Materials Reuse, Design for Deconstruction and Materials Reuse: Proceedings of the CIB Task Group 39 - Deconstruction Meeting, CIB World Building Congress, New Zealand (Vol. 272). Gainesville Florida: CIB / University of Florida.
[5] Chini, A. R. (2005), Deconstruction and materials reuse: an international overview. CIB.
[6] Bouvy, J. Demountable concrete structures: a challenge for precast concrete. Delft Univ Pr, 1985.
[7] Rice, E. (1978). Demountable multiple level building structures, Google Patents.
[8] Vambersky, J. N. J. A. (1994). "Precast concrete in building today and in the future." The structural Engineer 72(15).
[9] Lubliner, J., Oliver, J., Oller, S., and Onate, E. (1989). "A plastic-damage model for concrete." Int. J. Solids and Struct., 25(3), 299-326.
[10] Lee J., Fenves G.L., 1998. Plastic-damage model for cyclic loading of concrete structures. J. Eng. Mech. ASCE 124, 892–900.
[11] Kupfer, H., Hilsdorf, H. K., and Rusch, H. (1969). "Behavior of concrete under biaxial stresses." ACI J. 66(8), 656-666.
[12] Jankowiak, T., and Lodygowski, T (2005). "Identification of Parameters of Concrete Damage Plasticity Constitutive Model," Foundations of Civil and Environmental Engineering, No.6.
[13] Malm, R., 2006. Shear cracks in concrete structures sbujected to in-plane stresses. Lic. Thesis, Royal Institute of Technology (KTH), Stockholm.
[14] Carreira, D. and Chu, K. (1985), "Stress-strain relationship for plain concrete in compression", ACI Struct. J., 82(11), 797-804.
[15] CEB FIP MC 90 (1993), Design of Concrete Structures, CEB-FIP-Model-Code 1990, Thomas Telford, 1993.
[16] Elliott, K S (2002) Precast concrete structures. Elsevier Butterworth-Heinemann.
[17] Hibbit, D., B. Karlsson, et al. (2004). "ABAQUS Analysis User's Manual, version 6.5." Hibbit, Karlsson & Sorenson Inc., USA.
[18] Eurocode 3 (2005). BS EN 1993-1-8:2005-Design of steel structures -Part 1-8: Design of joints, British Standard Instituite
[19] Handbook, P. C. I. D. (2004). Precast Prestressed Concrete, Prestressed Concrete Institute, Chicago, IL.
[20] Hanus, F., G. Zilli, et al. (2011). "Behaviour of Grade 8.8 bolts under natural fire conditions—Tests and model." Journal of Constructional Steel Research 67(8): 1292-1298.
[21] BS EN ISO 898-1999, Mechanical properties of fasteners made of carbon steel and alloy steel — Part 1: Bolts, screws and studs.G. O. Young, "Synthetic structure of industrial plastics (Book style with paper title and editor)," in *Plastics*, 2nd ed. vol. 3, J. Peters, Ed. New York: McGraw-Hill, 1964, pp. 15–64.